Journal of the European Ceramic Society 21 (2001) 969–980

www.elsevier.com/locate/jeurceramsoc

Mechanical properties and tribology of Si_3N_4–TiB_2 ceramic composites produced by hot pressing and hot isostatic pressing

A.H. Jones [1], R.S. Dobedoe *, M.H. Lewis

Centre for Advanced Materials, Department of Physics, University of Warwick, Coventry CV4 7AL, UK

Received 4 February 2000; received in revised form 6 October 2000; accepted 10 October 2000

Abstract

Ceramic matrix composites containing TiB_2 as a particulate phase have been produced by hot pressing and hot isostatic pressing. The problems of the reactivity of TiB_2 with the Si_3N_4 matrix and with the sintering environment have been successfully addressed. A novel dual atmosphere sintering profile combined with low temperature hot pressing has been used to successfully produce fully dense materials. The effect of TiB_2 addition on mechanical properties has been investigated and the tribological behaviour of optimised compositions has been examined using a ball-on-disc apparatus. Wear coefficients and friction coefficients for Si_3N_4–TiB_2 composites have been measured and compared to monolithic Si_3N_4 materials. Composites containing TiB_2 show significant improvements in hardness, fracture toughness and wear whilst also exhibiting electrical conductivity.

Keywords: Fracture toughness; Hardness; Si_3N_4; TiB_2; Tribology

1. Introduction

Silicon nitride based ceramics are of particular interest for engineering applications because of their excellent combination of properties. Among these, the combination of high hardness and wear resistance makes them particularly attractive for tribological applications. However, to achieve widespread acceptance in the commercial sector there is still a need for materials with improved performance and properties.

The addition of conductive compounds such as TiC, TiN and TiB_2 to Si_3N_4 matrices to improve mechanical properties and to increase conductivity has been one approach taken.[1–3] Such an approach allows the production of conductive ceramics that can be shaped by electro-discharge machining (EDM) techniques leading to a material that can be machined to complex shapes without the need for expensive diamond machining.

This paper continues the study of Si_3N_4 and sialon based materials and the efforts to improve the hardness, toughness, wear resistance and conductivity by the use of particulate additions of TiB_2 to Si_3N_4 matrices.[3–5] Typical properties of Si_3N_4 and TiB_2 are shown in Table 1.[6] It should be noted that the commonly reported hardness of TiB_2 ($H_V = 33$ GPa)[7] is a microhardness for a load of 0.3 N. The macrohardness of TiB_2 (H_V 5–20 GPa)[8] has been used in this study when estimating the potential hardness improvement that can be achieved by adding TiB_2. In addition to the high hardness of TiB_2, its high elastic modulus and coefficient of thermal expansion (with respect to Si_3N_4) contribute to potential toughening mechanisms. In particulate composites, the potential toughening mechanisms have been identified as crack front-particle interaction, crack deflection, crack bridging, and residual stress fields caused by the mis-match in thermal expansion. All of the above may be operating and the dominating mechanisms depend upon the amount of TiB_2, the particle size and the type of Si_3N_4 matrix into which it is added. An in depth review of particulate-Si_3N_4 composites has been carried out by Gogotsi.[9]

One feature common to many of the studies of particulate-Si_3N_4 composites is the failure to produce fully dense materials, with many materials being $<98\%$ of the theoretical density (TD).[2,10–14] This is caused either

* Corresponding author.

E-mail address: r.s.dobedoe@warwick.ac.uk (R.S. Dobedoe).

[1] Now at Materials Research Institute, Sheffield Hallam University, Howard Street, Sheffield S1 1WB, UK.

0955-2219/01/$ - see front matter
PII: S0955-2219(00)00294-6

Table 1
Some typical properties of Si_3N_4 and TiB_2

Property	Si_3N_4 (β phase)	TiB_2
Crystal structure and lattice parameter (nm)	Hex. $a=b=0.775$, $c=0.291$	Hex. $a=b=0.303$, $c=0.323$
Density (ρ)	3.1–3.3 g/cc	4.52 g/cc
Hardness (H_V)	14–17 GPa	33 GPa (0.3 N), 20.8 GPa (5 N)
Toughness (K_{Ic})	3–8 MPa $m^{1/2}$	4.9–6.7 MPa $m^{1/2}$
Thermal expansion (α)	3.0–3.5 10^{-6}/K	6.6 (*a* and *b*), 8.7 (c) 10^{-6}/K
Elastic modulus (E)	290–320 GPa	500–575 GPa
Poisson's ratio (ν)	~0.27	~0.1
Electrical resistivity	$>10^{12}$ Ωcm	9×10^{-6} Ωcm
Thermal conductivity	15–43 W/mK	64 W/mK (20°C)

by porosity or by the presence of additional (low density) phases caused by reactions between the particulate and the matrix. The presence of either, even in small volumes, can offset any improvements brought about by the addition of the particulate phase and, at <95% TD, high reported values of E modulus, hardness or toughness should be treated with caution. The problems of poor densification and lower than expected properties have been addressed by increasing the sintering temperature.[2] However, while this approach works for Si_3N_4 ceramics in the absence of particulates, it merely exacerbates the problems in the presence of a reactive second phase. In order to achieve property improvements it is necessary, not only to add the second phase, but to avoid the problems outlined above by proper control of the starting compositions and sintering environment (for example: temperature, time, atmosphere).

The effect of particulate additions on the tribological performance of ceramics is complicated. Improved properties due to incorporation of a second phase do not necessarily result in improved wear performance. For example, the incorporation of TiB_2 into a SiC matrix increases the fracture toughness[15] and the incorporation of SiC into a Si_3N_4 matrix improves the bend strength and fracture toughness[14] but in neither case does this result in improved wear performance. However, the addition of either TiC[13,14] or TiN[16,17] to a silicon nitride matrix has been shown to substantially improve wear performance under conditions where tribochemical wear is dominant.

In order to assess the effect of TiB_2 addition on the tribological behaviour of silicon nitride, an investigation has been performed of the unlubricated sliding wear of a hot-pressed Si_3N_4-40 vol.% TiB_2 composite and a commercially produced silicon nitride against a silicon nitride ball. The test conditions were chosen to ensure that the primary wear mechanism for the silicon nitride/silicon nitride tribopair was tribochemical. A detailed discussion of the tribochemical wear mechanism for silicon nitride has been given by Fischer.[18] Limited tests have also been performed for both the silicon nitride and the Si_3N_4-40 vol.% TiB_2 composite against a hardened bearing steel counterbody.

2. Experimental procedure

2.1. Material production

The powders used to synthesise the composites were TiB_2 (H.C. Starck, Germany, Grade F) with a quoted particle size of D10 = 0.9–1.6 μm, D50 = 2–3.5 μm and a commercial sialon powder (containing 7 wt.% Y_2O_3 and 4 wt.% Al_2O_3) with a measured particle size of D50 = 0.3 μm. Some samples containing 40 vol.% TiB_2 were produced with a lower level of sintering additive (denoted by HP 40 vol.% TiB_2 rs). The silicon nitride matrix for the HP 40 vol.% TiB_2 rs consisted of α-Si_3N_4 (UBE, Japan, SN E-10) with 1 wt.% sintering additive in the form of a glass powder containing Y_2O_3:Al_2O_3:SiO_2 in the ratio 40:25:35 wt.%. The powders were ball milled in iso-2-propanol for 24 h in polyethylene jars, wet sieved through a 38 μm mesh, dried at 50°C and finally sieved through a 250 μm mesh to break up drying agglomerates. Green bodies were formed by uniaxially pressing at low pressure (~10 MPa) followed by wet-bag isopressing at 120 MPa. Green densities were in the range 50–60%. For hot pressing, the powders were added directly to the hot press die and compressed in situ at 30 MPa.

Hot pressing (HP) was carried out at temperatures between 1500 and 1700°C in an environmental hot press chamber where the atmosphere could be vacuum ($<1\times10^{-7}$ kPa) or 1 atmosphere (100 kPa) of argon or nitrogen. A vacuum of $\sim1\times10^{-7}$ kPa was achieved at 1000°C before any gases were admitted to the chamber. The powders were contained in graphite dies (50×50 mm or 25 mm diameter) lined with BN. A maximum pressure of 30 MPa was possible and densification was monitored via a displacement transducer attached to the hot press ram. Hot isostatic pressing (HIP) was carried out between 1550 and 1700°C on glass-encapsulated samples in a commercial apparatus (AC Cerama AB, Sweden) with a maximum applied pressure of 160 MPa of argon. The exact composition of the glass used for encapsulation, which is identical to that used to commercially HIP silicon nitride, is not available due to issues of commercial confidentiality.

2.2. Material characterisation

Crystalline phase composition was determined using X-ray diffraction (XRD) using Cu$K_{\alpha(1\text{ and }2)}$ radiation. The relative amount of α and β-Si_3N_4 was determined following the technique described by Gazzara and Messier.[19] The microstructure was examined using SEM, and EDX analysis was used to identify phases in the microstructure. Densities (ρ) were determined by the Archimedes water immersion method and were compared to theoretical densities calculated from the volumes of phases assumed to be present. Hardness and indentation fracture toughness were determined from 50 N Vickers diamond indentations carried out under conditions prescribed by the standards for the measurement of hardness (ASTM E384). Both hardness indent diagonals (2a) and the length of cracks (2c′) were measured by SEM, calibrated using a standard grid traceable to an NPL standard.[2] Great care was taken to accurately judge the ends of indents and crack tips by using high magnifications and back scattered electron (BSE) imaging. A HIPed Si_3N_4 (denoted as BGSN = bearing grade silicon nitride) produced by Toshiba, Japan, used commercially for ball bearings, was tested in parallel to act as a reference material. Its properties were H_V (50 N) = 15.5±0.5 GPa, K_{Ic} = 4.7±0.3 MPa $m^{\frac{1}{2}}$.

Vickers hardness (H_V) was calculated from $H_V = 1.8544\ P/2a^2$, where a is in μm and P is in N. Indentation fracture toughness (K_{Ic}) was calculated from crack length in two ways. The first was after Anstis et al.[20] [Eq. (1)] in order to compare results with those commonly found in the literature.

$$K_{Ic} = 0.016 \left(\frac{E}{H_V}\right)^{0.5} P(c')^{-1.5}\ \text{[MPa m}^{1/2}\text{]} \quad (1)$$

where E = elastic modulus (Pa), H_V = Vickers hardness (Pa), P = applied load (N), and $c' = \frac{1}{2}$ total crack-length (m).

The second method modifies an equation after Niihara et al.[21] [Eq. (2)] for median cracks to give a toughness parameter, TP, which is used for the assessment of Si_3N_4 ceramics in commercial applications:

$$TP = 10.281\ E^{0.4} P^{0.6}\ a^{-0.7}(c'/a)^{-1.5}\ \text{[MPa m}^{1/2}\text{]} \quad (2)$$

where a and c' are in μm, P is in kg and E is in GPa. It contains an empirically derived constant to compensate for the fact that, in Si_3N_4 ceramics, values of indentation fracture toughness are lower than those measured by non-indentation methods. TP yields values that can be compared with toughness data for Si_3N_4 materials tested by non-indentation techniques such as the single edge notched beam (SENB) and chevron notched beam (CNB) techniques.

The electrical resistivity measurements were performed on rectangular specimens with a Resistomat Type 2302 digital Ohmmeter (Burster Gernsbach Präzisionsmesstechnik), capable of measuring resistances from 0.1 μΩ up to 20 kΩ with a resolution of 0.1 μΩ. All measurements were made at room temperature.

The elastic moduli were calculated by measuring the speed of longitudinal and shear ultrasound waves transmitted through a disc of material. The bulk modulus (B), Poissons ratio (μ) and elastic modulus (E) can then be calculated from the following formulae (for isotropic materials):

$$B = V_T^2\rho, \quad \nu = \frac{1\text{-}2(V_T/V_L)^2}{2\text{-}2(V_T/V_L)^2}, \quad E = V_L^2\rho\frac{(1+\mu)(1-2\mu)}{(1-\mu)}$$

where ρ = density, V_L is the velocity of the longitudinal wave and V_T is the velocity of the transverse (or shear) wave.

The result can be compared with the theoretical modulus. Two methods were used to estimate the elastic modulus of a composite, the simple "rule of mixtures" approach which gives the Voigt–Reuss (VS) bounds and the Hashin and Shtrikman (HS) approach which uses a basic elastic energy theorem.[22]

VS model: $M = M_1V_1 + M_2V_2$ (lower bound), $\frac{1}{M} = \frac{V_1}{M_1} + \frac{V_2}{M_2}$ (upper bound) where M is either the bulk or shear modulus. Subscripts 1 and 2 denote the matrix and particle properties respectively. Young's modulus and Poisson's ratio are subsequently calculated from the bulk and shear modulus.

For the HS model:

$$\frac{M - M_1}{M_2 - M_1} = V_2\left[1 + \frac{V_1(M_2 - M_1)}{M_1 + H}\right]^{-1}$$

with $H = 4\mu_2/3$ or $H = 4\mu_1/3$ for the bounds on the bulk modulus and

$$H = \frac{\mu_2(9B_2 + 8\mu_2)}{6(B_2 + 2\mu_2)}; \quad H = \frac{\mu_1(9B_1 + 8\mu_1)}{6(B_1 + 2\mu_1)}$$

for the bounds on the shear modulus if $(\mu_2\text{–}\mu_1)(B_2\text{–}B_1) \geqslant 0$. For the case where $(\mu_2\text{–}\mu_1)(B_2\text{–}B_1) < 0$ these are replaced by

$$H = \frac{\mu_2(9B_1 + 8\mu_2)}{6(B_1 + 2\mu_2)}; \quad H = \frac{\mu_1(9B_2 + 8\mu_1)}{6(B_2 + 2\mu_1)}$$

[2] National Physical Laboratory, Teddington, UK.

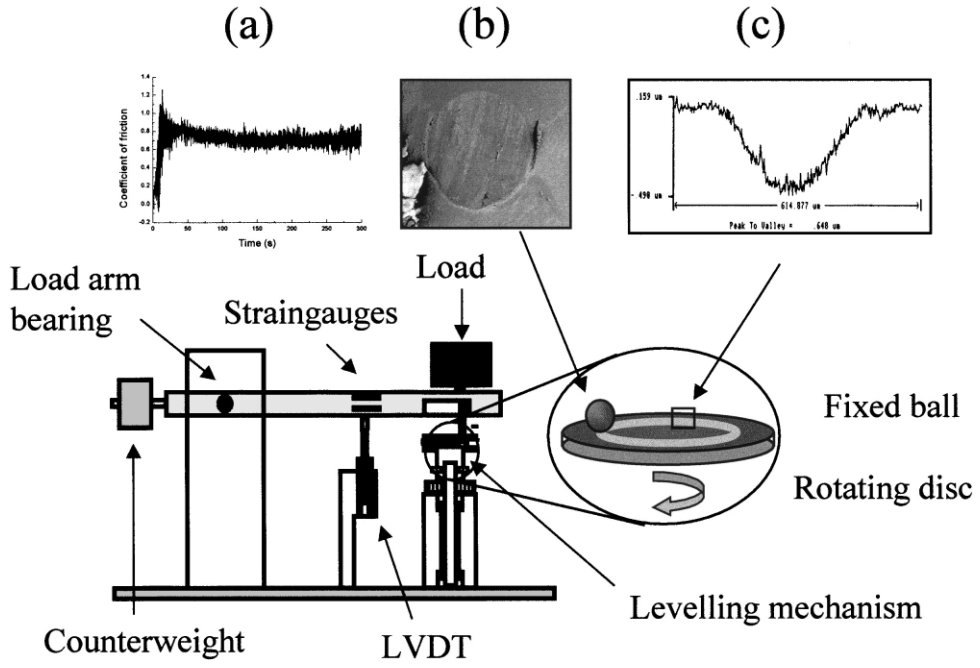

Fig. 1. Ball-on-disc tribometer illustrating capability to measure (a) coefficient of friction, (b) ball wear and (c), disc wear.

2.3. Wear testing

Wear tests were performed using an in-house designed ball-on-disc tribometer, shown schematically in Fig. 1. The fixed ball (or counterbody) was the upper specimen applied to a horizontal, rotating disc. The apparatus enabled the sample to be levelled prior to testing and allowed control of load, sliding speed, atmosphere and humidity. Standard test conditions are listed in Table 2. The apparatus and testing procedure did not differ significantly from that recommended by ASTM Standard Test Method for Wear Testing with a Pin-on-Disc Apparatus (G99-95a).

Prior to testing, all samples were cleaned ultrasonically in the following solutions: a commercial cleaning solution (MICRO-90: manufactured by International Products Corporation), acetone, a commercial cleaning solution (MICRO-90) and methanol. The ball and disc were then hot-plate dried to remove any volatile residues arising from the cleaning process. The ball counterbodies used were bearing grade silicon nitride (BGSN) or hardened bearing steel balls of 6.35 or 9.525 mm diameter. The BGSN used as both ball and disc samples is the same as that used as a reference standard in the measurement of H_V and K_{Ic}. The quoted properties of the hardened bearing steel balls were $E = 210$ GPa, H_V (50 N) = 7.8 GPa, $K_{Ic} = 12$–20 MPa $m^{1/2}$.

Table 2
Standard test conditions for wear testing

Parameter	Value
Load	5 N
Sliding speed	0.05 ms^{-1}
Atmosphere	Ambient laboratory air (~20°C)
Sliding distance	1000 m
Relative humidity	45–55%

The wear debris was analysed using TEM and EDX, which enabled the crystallinity and composition to be assessed. After the removal of loose debris the wear tracks were examined using SEM and EDX. Following a controlled cleaning procedure, using a vibrating nylon brush and a mild abrasive (a suspension of hydrated dicalcium phosphate) to remove the tribodebris from the wear track, a further SEM examination of the wear track was performed. This cleaning procedure was shown to have no observable effect on the microstructure outside the wear track, and hence its only effect was to remove debris generated during the wear test.

The diameter (d_b) of the wear scar on the ball was measured using optical microscopy and the wear volume of the ball (V_b) was estimated using the expression $V_b = \pi d_b^4/64R$, where R is the radius of the ball. The wear scar on the disc was measured using a Talysurf profilometer at eight points around the wear track both before and after the controlled cleaning process. The cross-sectional area of an individual profilometry trace was estimated by dividing the wear envelope into polygons whose area could be calculated easily. The wear volume of the disc (V_d) was estimated using the expression $V_d = A\pi d_d$, where A is the mean cross sectional area of the wear track and d_d is the diameter of the centre of the wear scar on the disc. Wear coefficients (units = $mm^3\ N^{-1}\ m^{-1}$) for the ball (k_b), the disc (k_d) and the combined total (k_t)

were calculated by dividing the volume removed by the applied load and the total distance slid

3. Results and discussion

3.1. HIPing

A range of compositions containing 0–100 vol.% TiB_2 were prepared by HIPing at 1550°C/60 min/160 MPa, 1650°C/90 min/160 MPa and 1700°C/120 min/160 MPa. The samples were totally enclosed in the glass encapsulant by ~1190°C and pressure was only applied after the samples had been encapsulated.

The percentage of theoretical density achieved by each composition at 1650 and 1700°C is shown in Fig. 2. The results for 1550°C/60 min are not shown, as they were identical to 1650°C.

The results for 1650°C demonstrated a simple relationship between increasing TiB_2 content and decreasing densification. However, increasing the temperature and time to 1700°C/120 min, which would normally improve the densification of Si_3N_4, resulted in a further decrease in the densification.

XRD and SEM carried out on these materials revealed that Si_3N_4 without TiB_2 additions achieved theoretical density, forming a microstructure of β-Si_3N_4 grains and an amorphous intergranular phase. However, the failure of materials containing TiB_2 to achieve theoretical density was not caused simply by lack of densification (i.e. residual porosity) but by a complex interaction between Si_3N_4 and TiB_2 at high temperatures.

The presence of a TiN phase was detected by XRD (Fig. 3). SEM and EDX verified the presence of areas of TiN associated with TiB_2 particles (Fig. 4). The presence of BN in the microstructure was confirmed by the use of EDX (Fig. 5). BN cannot be detected by XRD in the presence of β-Si_3N_4, due to its primary peak overlapping with the β-Si_3N_4 (200) peak. The dark appearance of BN under both electron and optical microscopy and its propensity to be pulled out or preferentially polished can lead to it being wrongly interpreted as porosity.

A possible explanation for the formation of TiN is via the reaction:

$$4TiB_2 + 3Si_3N_4 \rightarrow 4TiN + 8BN + 9Si, \quad \Delta G = -25\,\text{kJ mol}^{-1}(1500\,\text{K}) \tag{3}$$

Or alternatively Si_3N_4 decomposes forming Si and N_2 gas which then reacts with the TiB_2 forming TiN and BN [Eq. (4)].

$$2TiB_2 + 3N_2(g) \rightarrow 2TiN + 4BN, \quad \Delta G \cong -100\ \text{kJ mol}^{-1}(1880\,\text{K}, 1\,\text{atm}\,N_2) \tag{4}$$

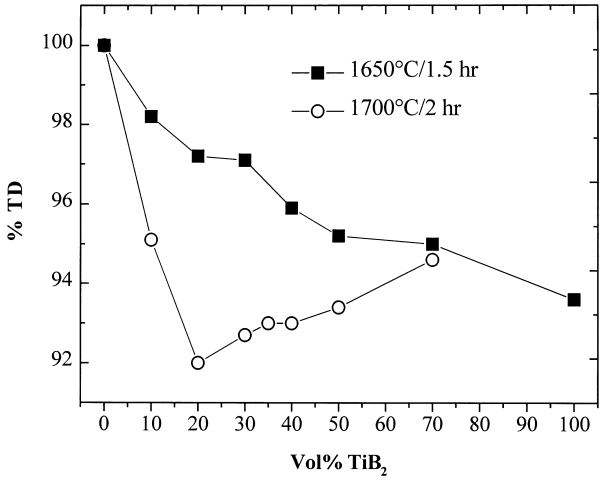

Fig. 2. Densification of Si_3N_4 composites containing 0–100 vol.% TiB_2 after HIPing at 1650°C/1.5 h (■) and 1700°C/ 2 h (○) at 160 MPa.

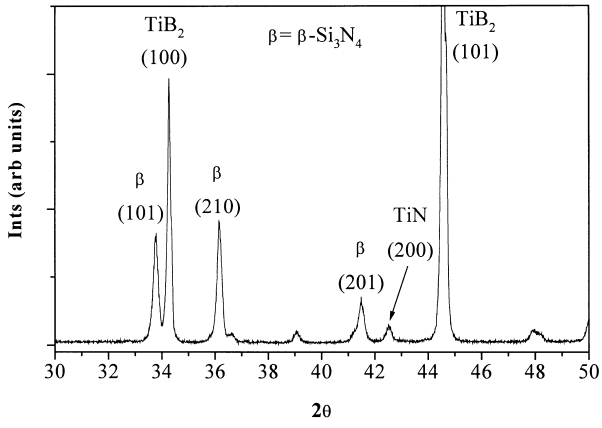

Fig. 3. XRD spectrum from Si_3N_4/40 vol.% TiB_2 HIPed at 1650°C/1.5 h.

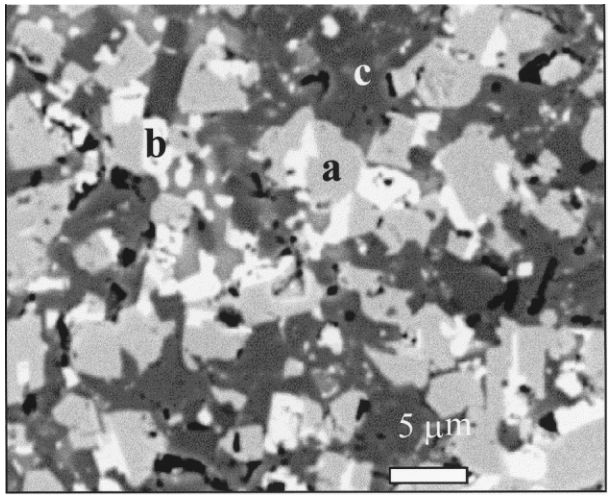

Fig. 4. SEM BSE micrograph of 1700°C HIPed material (40 vol.% TiB_2). a = TiB_2, b = TiN, c = β-Si_3N_4. Darkest regions are porosity or BN.

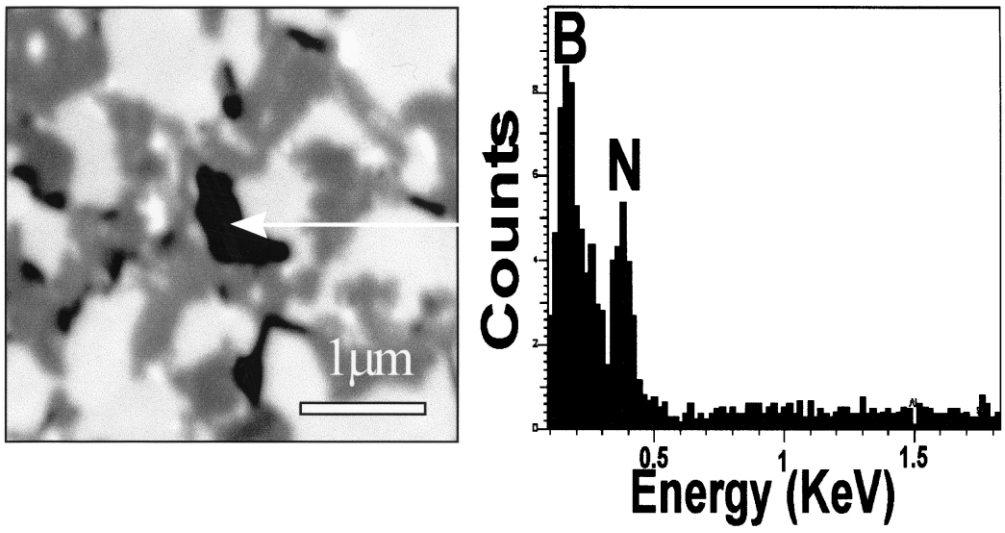

Fig. 5. EDX analysis of dark inclusion in microstructure showing it to be BN.

However, Si or unexpected Si containing phases (e.g. titanium silicides) were not detected at temperatures below 1750°C which suggests that the above mechanisms alone do not adequately explain the formation of TiN. Other work has shown that the above reactions [Eqs. (3) and (4)] form an interfacial reaction zone of TiN around TiB_2 particles.[10] However, HIPing at 1700°C/120 min formed zones of TiN which appear to nucleate and grow along crystallographic planes *within* the TiB_2 particles (Fig. 4). This indicates a different mechanism from that described by Shew et al.[10] It is proposed that the liquid phase formed at the sintering temperature by the additives (Y_2O_3, Al_2O_3 and SiO_2) acts as a flexible receptor for dissolved ions. It is the activity of various species in this phase and the kinetics of the migration of ions through this phase that controls the rate and type of reaction that occurs. This is supported by the observation that areas of TiN were not formed adjacent to areas of BN in the microstructure (Fig. 4), suggesting that they were nucleated from the liquid at separate sites. However, the determination of the exact mechanisms requires further work.

The samples HIPed at 1550°C showed similar properties, microstructure and phase composition to those HIPed at 1650°C. It appears that the 1550°C samples had seen temperatures close to 1650°C. The higher than expected temperature in the HIPing apparatus may have been due to the use of temperatures below normal operating conditions.

3.2. Hot pressing

Conventional hot pressing of Si_3N_4 takes place under a nitrogen atmosphere to suppress decomposition at high sintering temperatures. However, as previously mentioned [Eq. (4)] a nitrogen atmosphere could react with TiB_2 forming TiN and BN. In order to avoid this, a hot pressing procedure was developed to minimise such reactions. Use of an argon atmosphere until the sample achieved closed porosity avoided the formation of TiN. Once closed porosity occurred the atmosphere was changed to nitrogen to avoid the decomposition of Si_3N_4. Any reactions were then limited to the very outer layer of the specimen, which was removed by normal sample preparation. Since only 1 atm of nitrogen could be applied in the hot press, temperatures used were $<$ 1700°C to avoid decomposition.

Hot pressing was carried out at 1500, 1550, 1600, 1650 and 1670°C for 60 min at 30 MPa applied pressure with the above mentioned dual atmosphere cycle. The procedure used is demonstrated in Fig. 6. Work on electro-conductive ceramics indicates that >35 vol.% of particulate additions are required to provide an interconnecting network, necessary for high conductivity.[23] Considering this and the results for fracture toughness in HIPed materials (see below), all hot press compositions contained 40 vol.% TiB_2.

Decreasing the hot pressing temperature to as low as 1500°C resulted in densities equal to the theoretical (99.5% TD, $\rho = 3.727$ g/cc) for a 40 vol.% TiB_2 composite. Hot pressing at 1500°C of the silicon nitride matrix material with no TiB_2 addition did not result in a dense material (90% TD, $\rho = 2.934$ g/cc) and thus it is clear that the addition of TiB_2 actually aids the densification of the composites at low temperatures. The use of lower hot pressing temperatures has also reduced the formation of TiN and BN. Hot pressing at 1500°C produced a dual phase matrix of α-Si_3N_4 and β-Si_3N_4 as shown by XRD (Fig. 7). The effect of temperature on the density and α-Si_3N_4 content of 40 vol.% TiB_2 composites is shown in Table 3. The low temperature reduces the transformation to β-Si_3N_4 and forms a matrix with a small grain size. The TiB_2 is homogeneously distributed in the matrix and retains the small particle size

of the starting powder. Any apparent porosity is assumed to be polishing damage caused by the removal or preferential polishing of BN particles. An image of the microstructure is shown in Fig. 8 and, when compared with Fig. 4, clearly shows that the formation of TiN and BN had been significantly reduced. Due to the small grain size and the contrast of the TiB_2 it is extremely difficult to clearly image the matrix microstructure but it is apparent that the average grain size is <2 μm.

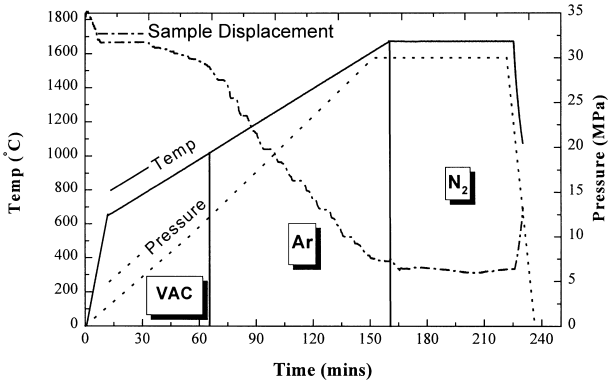

Fig. 6. Hot press time/temperature/pressure/atmosphere cycle with sample displacement data from a typical hot press run.

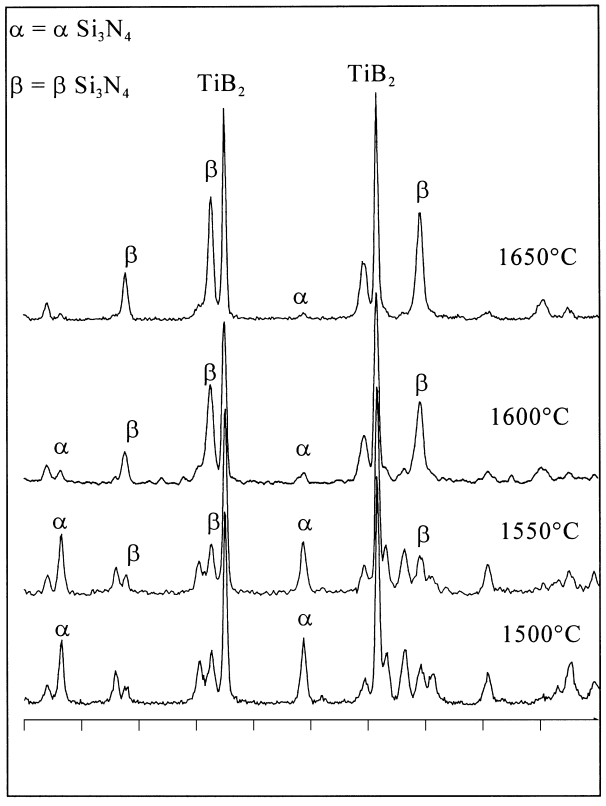

Fig. 7. XRD from samples hot pressed at different temperatures. More α-Si_3N_4 is present in lower temperature materials.

3.3. Hardness and toughness

3.3.1. HIPed materials

The effect of TiB_2 content on hardness and indentation fracture toughness of the materials HIPed at 1650°C is shown in Fig. 9. The hardness was seen to initially drop as the addition of TiB_2 reduced densification at 1650°C (see Fig. 2). The hardness then rose with increasing TiB_2 content showing that TiB_2 contributes to the hardness of the composite despite the presence of porosity and other phases. At this temperature, the magnitude of the hardness increase due to TiB_2 addition is partially offset by the increase in porosity, TiN and BN.

For composites HIPed at 1650°C, a peak in fracture toughness of $K_{Ic}=5.8\pm0.2$ MPa $m^{\frac{1}{2}}$ ($TP=8.0$ MPa $m^{\frac{1}{2}}$) was observed for 40 vol.% TiB_2. Observation of crack paths from the corners of Vickers indentations showed both deflection around particles and transgranular fracture of the TiB_2 (Fig. 10).

3.3.2. Hot pressed materials

Hot pressed materials containing 40 vol.% TiB_2 exhibit an increase in hardness with decreasing hot pressing temperature. Table 3 and Fig. 11 show the effect of hot pressing temperature on density, α-Si_3N_4 content, hardness and toughness. The optimum hardness/density combination is produced at 1500°C with 99.5% of TD ($\rho=3.726$ g/cc) and $H_V=17.4$ GPa. This is a significant improvement in hardness over the reference material ($H_V=15.5$ GPa). The higher hardness of α-Si_3N_4 compared to β-Si_3N_4, the reduction in TiN and BN content, the decrease in porosity and the reduced grain size all contribute to the improved hardness.

Toughness in Si_3N_4 ceramics is usually lowered by the presence of small equiaxed α grains, as it is the elongated β grains that give rise to the crack deflection toughening mechanism. However, the toughness of hot pressed TiB_2 containing composites is maintained in the absence of β-Si_3N_4 with $K_{Ic}=4.9$ MPa $m^{\frac{1}{2}}$ ($TP=6.4$ MPa $m^{\frac{1}{2}}$). It is proposed that the presence of TiB_2 contributes

Table 3
Properties of composites containing 40 vol.% TiB_2 hot pressed at different temperatures

Temperature (°C)	ρ (g/cc)	% TD	% α-Si_3N_4	H_V (GPa)	K_{Ic} (MPa $m^{\frac{1}{2}}$)	TP (MPa $m^{\frac{1}{2}}$)
1500	3.726	99.5	0.62	17.4	4.9	6.9
1550	3.693	98.6	0.56	16.4	5.0	6.92
1600	3.661	97.7	0.17	16.0	4.6	6.4
1650	3.640	97.2	<0.05	15.8	4.6	6.4

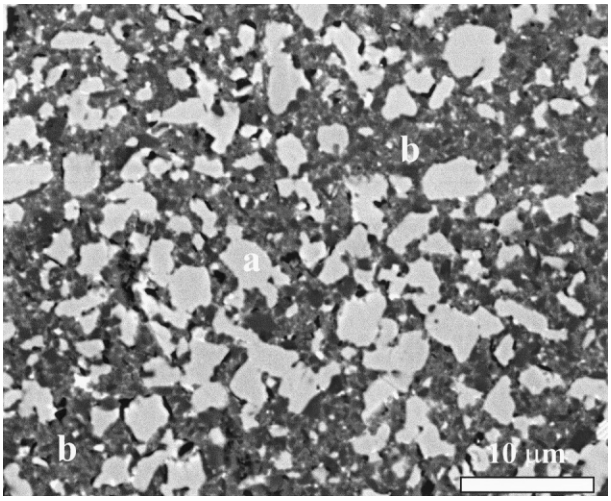

Fig. 8. SEM BSE image of the microstructure of a 40 vol.% TiB_2–Si_3N_4 composite hot pressed at 1500°C/60 min/30 MPa. a = TiB_2, b = matrix (α-Si_3N_4 and β-Si_3N_4).

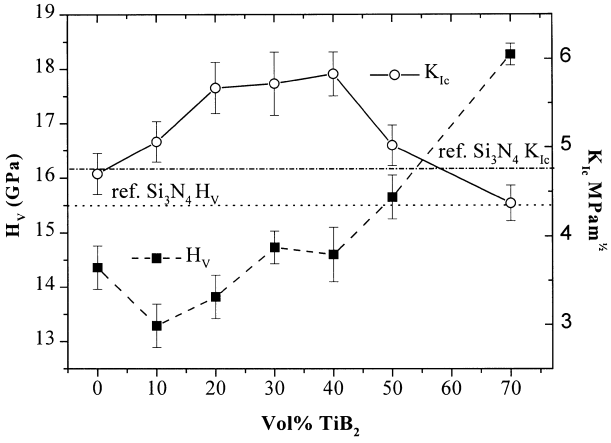

Fig. 9. Variation of hardness (■) and indentation fracture toughness (○) with TiB_2 content of HIPed materials (1650°C/90 min/160 MPa). Dotted lines indicate values for the reference HIPed Si_3N_4 material.

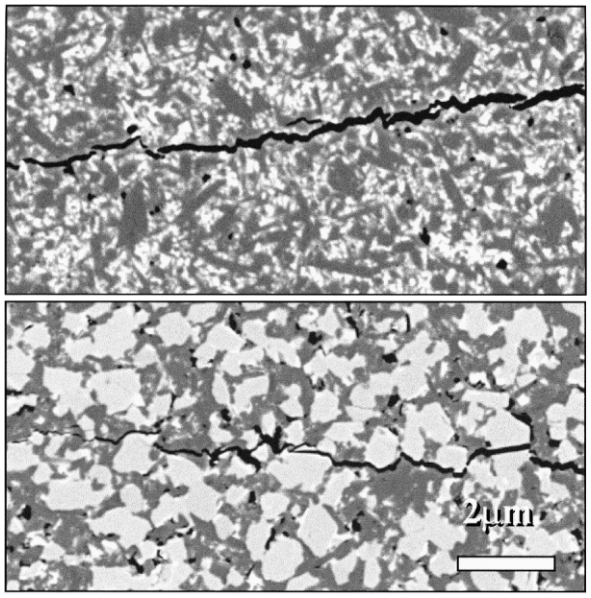

Fig. 10. SEM back scattered electron images of crack paths through (a) HIPed Si_3N_4 and (b) HIPed Si_3N_4–40 vol.% TiB_2.

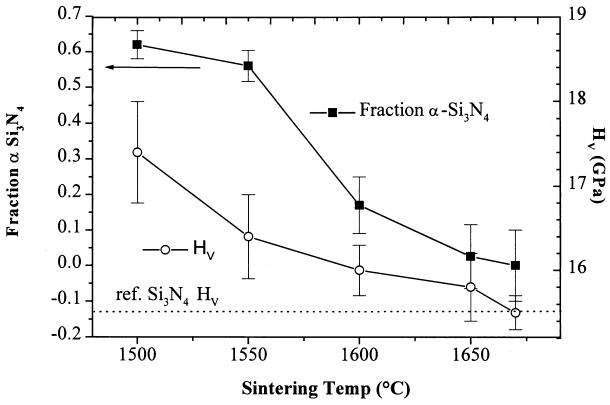

Fig. 11. Variation of α-Si_3N_4 (■) and H_V (○) with hot pressing temperature of 40 vol.% TiB_2 material. Dotted line indicates the reference HIPed Si_3N_4 hardness.

to toughening in the ways outlined above but that this is offset by increasing α-Si_3N_4 content.

The difference between toughness for HIPed and HP materials containing similar amounts of TiB_2, is possibly due to the difference in α-Si_3N_4 content caused by the shorter hot pressing time at 1650°C. In HIPed materials all the α-Si_3N_4 has been transformed to β-Si_3N_4 and some growth of the β grains may have occurred, contributing to the toughening. It is also possible that the property of the intergranular glass varies between the two materials and that this affects the toughness.

3.4. Electrical conductivity and elastic modulus

Initial assessment of the conductivity of the composites showed levels of conductivity significantly higher than for Si_3N_4. Two samples, hot pressed with 40 vol.% TiB_2, were measured, one containing a lower level of sintering additive (denoted by HP 40 vol.% TiB_2 rs). They exhibit values of electrical conductivity that allow EDM to be easily performed (Table 4). The higher value for the sample with reduced sintering aid indicates that the nature of the residual intergranular phase affects electrical properties.

The E modulus and Poisson's ratio of a material containing 40 vol.% TiB_2 were measured as $E = 365$ GPa±30 GPa and $\nu = 0.19 \pm 0.01$. When consideration is given to the effect of porosity on elastic modulus[24] (~3% in the sample measured) then $E_{dense} = 387 \pm 30$ GPa and the experimental value is seen to lie close to the lower HS bound (Fig. 12). This indicates that there is no significant spontaneous microcracking in the presence of TiB_2. Microcracking results in a measurable reduction in the E modulus[25] without raising the measured porosity. The stresses produced on cooling due to the difference in thermal expansion of Si_3N_4 and TiB_2

Table 4
Electrical conductivity for hot pressed composites compared with the TiB_2 and conventional Si_3N_4

Sample	Conductivity (Ω^{-1} cm^{-1})	Resistivity (Ωcm)
Conventional Si_3N_4[23]	$< 10^{-13}$	$> 10^{12}$
HP 40 vol.% TiB_2	3×10^{3}	335×10^{-6}
HP 40 vol.% TiB_2 rs[a]	9×10^{3}	116×10^{-6}
TiB_2	111×10^{3}	9×10^{-6}

[a] rs = reduced sintering aid.

are partially relieved by the presence of a viscous phase formed by the oxide sintering additives (Y_2O_3, Al_2O_3 and SiO_2) and hence microcracking is not expected.

3.5. Wear

The results from wear tests are discussed in terms of each tribopair.

3.5.1. BGSN ball/BGSN disc

For the BGSN/BGSN tribopair under ambient humidity (40–50% RH), the wear tests resulted in fine, white powder debris and wear scars on both the disc and the ball. Optical microscopy revealed tribofilm adherent on areas of the disc and ball scars. TEM analysis of the debris confirmed the amorphous nature of the debris (no crystallinity observed) and revealed that the nitrogen content was below the EDX detection threshold. TEM EDX spectra of Si_3N_4 powder taken under similar conditions reveals the EDX detection threshold for nitrogen to be 0.7 wt.%. The absence of crystalline wear debris and their low nitrogen content suggest that microfracture is not a significant wear mechanism and that tribochemical wear is dominant.

The wear debris were thin, amorphous films and cylinders or rolls of debris similar to those reported by other workers[16] to be hydroxylated silicon oxide (Fig. 13). Measurements of the disc wear showed little difference before and after the final cleaning procedure. The coefficient of friction (μ) for BGSN on BGSN was 0.50±0.05.

The variation of disc wear coefficients (k_d) with humidity for the BGSN material after cleaning are shown in Fig. 14. The coefficient of friction and the wear coefficients are consistent with the consensus of results reported in the literature for similar test conditions.[6,26]

3.5.2. BGSN ball/ Si_3N_4–40 vol % TiB_2 disc

The BGSN/Si_3N_4–TiB_2 tribopair resulted in similar low nitrogen content, amorphous debris but with reduced formation of cylindrical wear debris. Typical secondary and back-scattered electron micrographs of the disc wear track are shown in Fig. 15(a) and (b). In back scattered electron mode [Fig. 15(b)] the outline

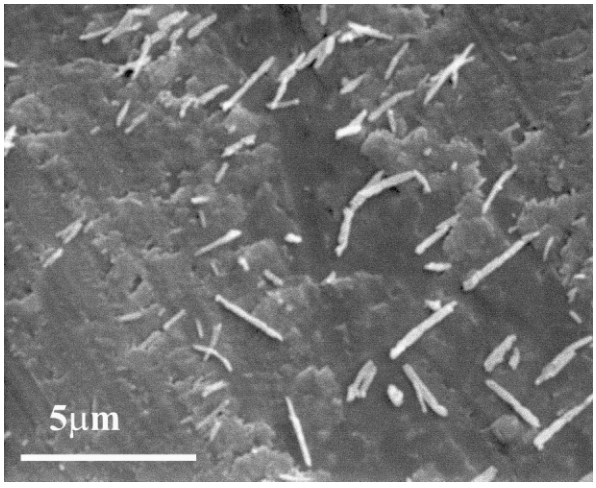

Fig. 13. SEM image of cylindrical wear debris produced from a BGSN–BGSN tribopair under standard conditions.

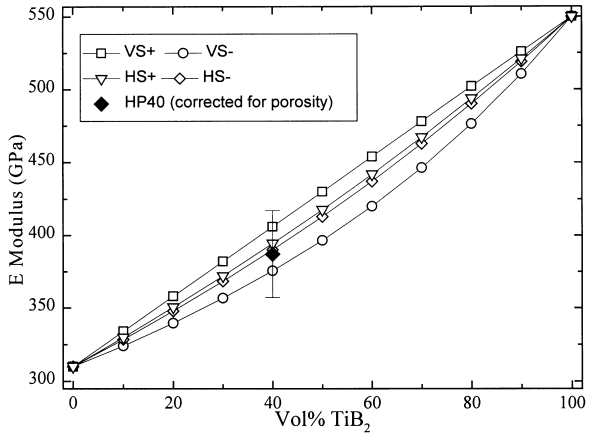

Fig. 12. Calculated VR and HS bounds for E modulus of hot pressed Si_3N_4–40 vol.% TiB_2 composites and measured E (◆).

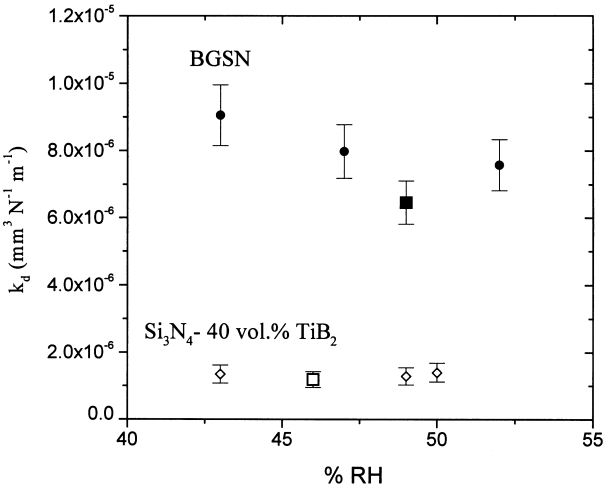

Fig. 14. Variation of disc wear coefficients (k_d) with humidity for BGSN (●) and Si_3N_4–40 vol.% TiB_2 (◇) discs against BGSN balls. The points (■) and (□) represent the use of a larger (9.35 mm) diameter ball. Conditions: 1 km, 5 N, 0.05 ms^{-1}, 20°C.

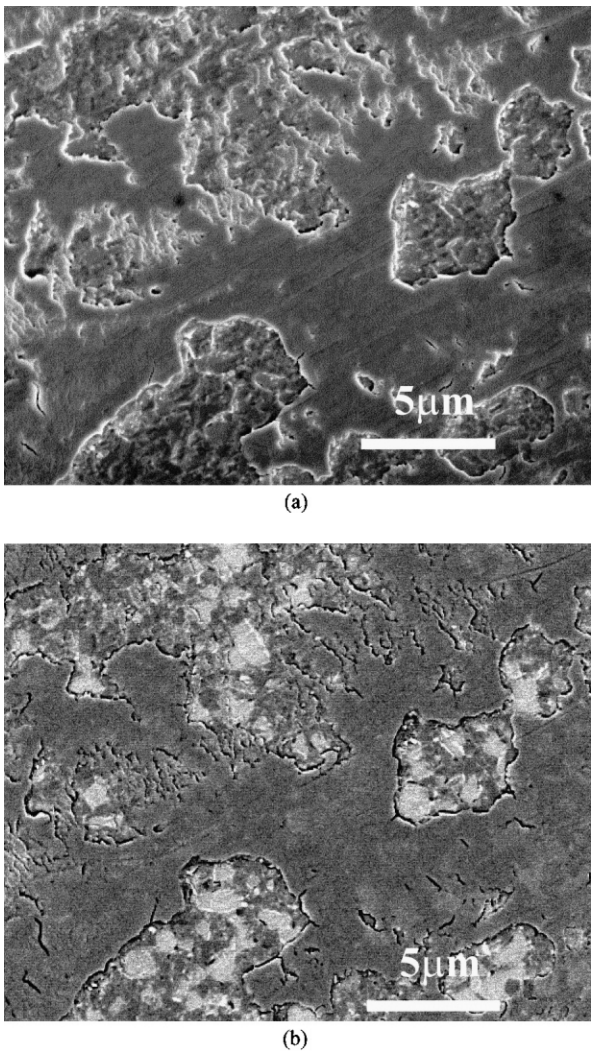

Fig. 15. SEM images of the wear track for BGSN ball on Si_3N_4–40 vol.% TiB_2: (a) secondary electron image and (b) back scattered electron image.

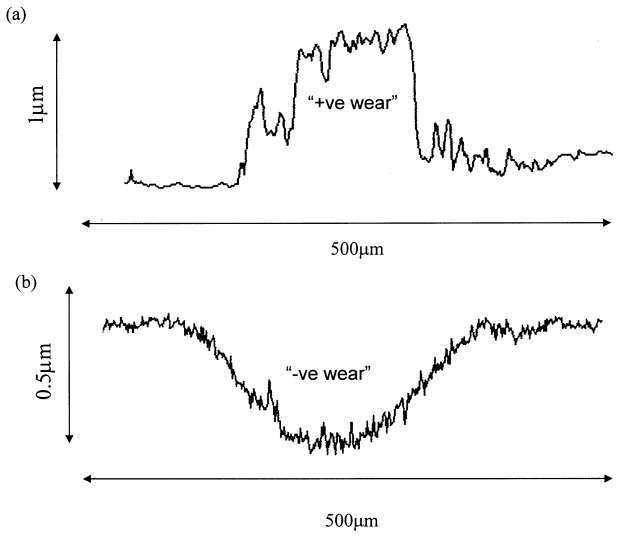

Fig. 16. Typical profilometry traces from the wear track of a Si_3N_4–40 vol.% TiB_2 material: (a) before and (b) after cleaning.

microstructure of the composite could be seen through the tribofilm. Measurement of the Si_3N_4–TiB_2 disc wear could only be performed after the final cleaning procedure due to more strongly adherent wear debris. A typical profilometer trace before and after the final cleaning procedure is shown in Fig. 16. Prior to this measurement some areas of the wear track would result in 'positive' wear due to the presence of wear debris/tribofilm on the surface [Fig. 16(a)]. The coefficient of friction for the Si_3N_4–TiB_2 disc was 0.55±0.05, slightly higher than that for the matched BGSN tribopair although the difference is not necessarily significant.

The wear coefficients (k_d) for BGSN and Si_3N_4–40 vol.% TiB_2 discs sliding against a BGSN ball as a function of humidity are shown in Fig. 14. The small scatter in the measured disc wear indicates excellent reproducibility of both the testing and measurement procedure. In the ambient humidity range (45–55% RH) the disc wear of the Si_3N_4–40 vol.% TiB_2 was lower by a factor of five. The wear coefficient of the BGSN ball was similar for both tribopairs ($4–5\times10^{-6}$ $mm^3\ N^{-1}\ m^{-1}$).

Wear tests performed at low humidity (<15% RH) using a BGSN/Si_3N_4–40 vol.% TiB_2 tribopair resulted in fine grey wear debris and an order of magnitude increase in the disc wear coefficient (k_d). TEM analysis of the debris revealed partially crystalline debris with detectable levels of nitrogen, indicating that microfracture was an active wear mechanism. Low humidity has been reported to result in similar increases in wear and changes in wear mode for matched silicon nitride/silicon nitride tribopairs under similar conditions.[27] This confirms that, for the Si_3N_4–40 vol.% TiB_2 composite, water vapour is actively involved in the formation of the tribofilm.

3.5.3. Steel ball/BGSN disc and steel ball/Si_3N_4–40 vol.% TiB_2

Wear against the steel ball was also tribochemically dominated with discs of Si_3N_4–40 vol.% TiB_2 displaying a fivefold reduction in wear compared to those of BGSN. The Si_3N_4–40 vol.% TiB_2 composite does however result in increased wear of the steel counterbody when compared to the steel ball/BGSN tribopair. The improved wear performance of the Si_3N_4–40 vol.% TiB_2 composite is summarised in Table 5.

The extent to which the improved tribological performance can be attributed to the superior mechanical properties (H_V, K_{Ic}) or to the superior protective properties of the oxide tribofilm is not yet clear. However, similar improvements in the tribochemical wear performance of silicon nitride containing TiC[13] and TiN[16] suggest that the presence of titanium may be primarily responsible for a beneficial modification to the tribofilm/tribochemistry. No reduction in the coefficient of

Table 5
Comparison of disc, ball and total wear rates (k_d, k_b, k_t respectively) for various tribopairs

Tribopair		Wear coefficient (k)-$\times 10^{-6}$ mm^3 N^{-1} m^{-1}		
Ball	Disc	Ball (k_b)	Disc (k_d)	Total (k_t)
Si_3N_4 (BGSN)	Si_3N_4 (BGSN)	4.1±0.4	7.7±0.8	11.8±1.2
Si_3N_4 (BGSN)	Si_3N_4–40 vol.%TiB_2	5.0±0.5	1.6±0.2	6.6±0.7
Steel	Si_3N_4 (BGSN)	0.5±0.1	6.1±0.6	6.6±0.7
Steel	Si_3N_4–40 vol.%TiB_2	1.1±0.1	1.3±0.2	2.4±0.3

friction is observed when TiB_2 is present indicating that the improved wear performance is not related to any lubricating role of either the TiB_2 or the resulting tribofilm. High temperature wear tests of silicon nitride containing either TiN[16] or TiC[13] have been reported to result in a lower coefficient of friction and improved wear performance compared to monolithic silicon nitride. It is anticipated that similar performance improvements at elevated temperatures would be observed from silicon nitride-TiB_2 composites.

4. Summary

Si_3N_4–TiB_2 composites were produced by both hot isostatic pressing and hot pressing under various conditions. In order to realise the improvements in properties that the addition of TiB_2 to Si_3N_4 can provide it was necessary to avoid the formation of TiN and BN and to achieve full density. This was only possible by lowering the sintering temperature to 1500°C where the presence of TiB_2 (or its oxides) aided densification. The composition, phase content and properties of the Si_3N_4 matrix influence the properties almost as much as the addition of TiB_2.

The use of low hot pressing temperatures has resulted in a fully dense, α-Si_3N_4/β-Si_3N_4 matrix with a small grain size. Hot pressed composites containing 40 vol.% TiB_2 in such a matrix exhibited improved hardness and toughness ($H_V = 17.4$ GPa, $K_{Ic} = 4.9$ MPa m$^{\frac{1}{2}}$) and a higher E modulus ($E = 365 \pm 35$ GPa) when compared to a commercial HIPed Si_3N_4. The mismatch in thermal expansion between the constituent phases did not result in microcracking, partially due to the presence of a viscous, intergranular phase.

For HIPed materials, hardness increased with TiB_2 content and a peak in toughness ($K_{Ic} = 5.8$ MPa m$^{\frac{1}{2}}$) was seen at a level of 40 vol.% TiB_2. At this level the particulates form an inter-connecting network which increased the electrical conductivity to a level where EDM is a possibility. A separate study, soon to be published, has examined the shaping of these materials by the application of novel EDM methods. The effect of TiB_2 on thermal properties could also lead to improved performance in applications such as high speed cutting and other tribological applications.

When compared to a commercial bearing grade silicon nitride, a silicon nitride with a high α-Si_3N_4 content matrix containing 40 vol.% TiB_2 displayed a fivefold improvement in unlubricated sliding wear performance against both a commercial silicon nitride and a steel counterbody.

The addition of TiB_2 to silicon nitride resulted in a beneficial modification of the tribochemistry and a tribofilm that was more effective at protecting both the composite disc and the ball from wear.

Acknowledgements

This research was carried out as part of a BRITE-EURAM project (BE96-3356 Contract No.: BRPR-CT96-0304). Electrical conductivity measurements were carried out by Jef Vleugels at MTM, Katholieke University, Leuven, Belgium. The bearing grade silicon nitride reference material was supplied by Dr. Robin Cundill of SKF Engineering and Research Centre, The Netherlands.

References

1. Hong, H., Lumby, R. J. and Lewis, M. H., TiN/Sialon composites via in-situ reaction sintering. *J. Eur. Ceram. Soc.*, 1993, **11**, 237–239.
2. Yoo, S. E., Rhee, M. H., Kim, H. J. and Lee, S. W., Mechanical properties of hot-pressed Si_3N_4–TiC composites. *Key Eng. Materials*, 1999, **161–163**, 321–324.
3. Jones, A. H., *Synthesis and tribology of sialon/TiB_2 composites*. PhD thesis, University of Warwick, Coventry, UK, 1997.
4. Jones, A. H., Lumby, R. J., Hong, F. and Lewis, M. H., Ceramic matrix composites via in-situ reaction sintering. *Br. Ceram. Proc.*, 1994, **53**, 221–232.
5. Jones, A. H., Dobedoe, R. S., Lewis, M. H. and Lumby, R. J., Sialon/TiB_2 ceramic composites: synthesis, properties and tribology. *Br. Ceram. Proc.*, 1999, **59**, 133–149.
6. Adapted from "Properties of Nitrides". In *Engineering Materials Handbook*, Vol. 4. Ceramics and Glasses, ASM International, 1994.
7. Cutler, R. A., Engineering properties of borides. In *Engineering Materials Handbook*. Vol. 4. Ceramics and Glasses, ASM International, 1994.
8. Chung, S. K., Fracture characterisation of armour ceramics. *Am. Ceram. Soc. Bull.*, 1990, **69**(3), 358–366.
9. Gogotsi, Y. G., Review: particulate silicon nitride-based composites. *J. Mater. Sci.*, 1994, **29**, 2541–2556.

10. Shew, B.-Y. and Huang, J.-L., Investigation of the chemical reactions in TiB_2/Si_3N_4 composites. *Mater. Sci. Eng*., 1992, **A159**, 127–133.
11. Huang, J.-L., Kuo, F.-J. and Chen, S.-Y., Investigation of the microstructure and crack behaviour in hot-pressed TiB_2–Si_3N_4 composites. *Mater. Sci. Eng*., 1994, **A174**, 157–164.
12. Huang, J.-L., Lee, M.-T. and Lu, H.-H., Microstructure, chemical reaction and mechanical properties of TiC/Si_3N_4 and TiN-coated TiC/Si_3N_4 composites. *J. Mater. Sci*., 1996, **31**, 4899–4906.
13. Blanchard, C. R. and Page, R. A., Effect of silicon carbide whisker and titanium carbide particulate additions on the friction and wear behaviour of silicon nitride. *J. Am. Ceram. Soc*., 1990, **73**(11), 3442–3452.
14. Page, R. A., Blanchard-Ardid, C. R. and Wei, W., Effect of particulate additions on the contact damage resistance of hot pressed silicon nitride. *J. Mater. Sci*., 1998, **23**, 946–957.
15. Ajayi, O. O., A. Erdemir, A., Lee, R. H. and Nichols, F. A., Sliding wear of silicon carbide-titanium diboride ceramic-matrix composite. *J. Am. Ceram. Soc*., 1993, **76**(2), 511–517.
16. Skopp, A., Woydt, M. and Habig, K.-H., Tribological behaviour of silicon nitride materials under unlubricated sliding between 22 and 1000°C. *Wear*, 1995, **181–183**, 571–580.
17. Imada, Y., Kanamura, K., Honda, F. and Nakajima, K., The tribological reaction accompanying friction and wear of silicon nitride containing titanium nitride. *A.S.M.E. Trans., J. Trib*., 1992, **114**, 230–235.
18. Fischer, T. E. and Mullins, W. M., Chemical aspects of ceramic tribology. *J. Phys. Chem*., 1992, **96**, 5690–5701.
19. Gazzara, C. P. and Messier, D. R., Determination of phase content of Si_3N_4 by X-ray diffraction analysis. *Am. Ceram. Soc. Bull*., 1977, **56**(9), 777–780.
20. Anstis, G. R., Chantikul, P., Lawn, B. R. and Marshall, D. B., Indentation techniques for measuring toughness of ceramics. *J. Am. Ceram. Soc*., 1981, **64**, 539.
21. Niihara, K., Morena, R. and Hasselman, D. P. H., Evaluation of K_{Ic} of brittle solids by the indentation method with low crack-to-indent ratios. *J. Mater. Sci*., 1982, 13–16.
22. Watt, J. P., Davies, G. F. and O'Connell, R. J., Elastic properties of composite materials. *Rev. Geophys. Space Phys*., 1976, **14**(4), 541–563.
23. Kamijo, E., Honda, M., Higuchi, M., Takeuchi, H. and Tanimura, T., Electrical discharge machinable Si_3N_4 ceramics. *Sumitomo Electrical Technical Review*, No. 24, January 1985, pp. 183–190.
24. MacKenzie, J. K., The elastic constants of a solid containing spherical holes. *Proc. Phys. Soc. (Lond)*., 1950, **B63**, 2.
25. Pan, M. J., Hoffman, P. A., Green, D. J. and Hellmann, J. R., Elastic properties and microcracking behaviour of particulate titanium diboride-silicon carbide composites. *J. Am. Ceram. Soc*., 1997, **80**(3), 692–698.
26. Dong, X. and Jahanmir, S., Wear transition diagram for silicon nitride. *Wear*, 1993, **165**, 169–180.
27. Fischer, T. E. and Tomizawa, H., Interaction of tribochemistry and microfracture in the friction and wear of silicon nitride. *Wear*, 1985, **105**, 29–45.